Electronic Supplementary Material (ESI) for Journal of Materials Chemistry C.

Supporting information

Magnetic transitions and isotropic versus anisotropic magnetic behaviour of $[CH_3NH_3][M(HCOO)_3]$ M = Mn^{2+}, Co^{2+}, Ni^{2+}, Cu^{2+} metal-organic perovskites

B. Pato-Doldán,‡[a†] L. C. Gómez-Aguirre,‡[a] A. P. Hansen,[b] J. Mira,[c] S. Castro-García,[a] M. Sánchez-Andújar,[a] M. A. Señarís-Rodríguez,[a] V. Zapf[b] and J. Singleton[b]

[a.] *QuiMolMat Group, CICA, Department of Fundamental Chemistry, Faculty of Sciences, University of A Coruña, Campus A Coruña, 15071 A Coruña, Spain.*
[b.] *National High Magnetic Field Laboratory, Los Alamos National Laboratory, Los Alamos, New Mexico 87545, United States.*
[c.] *Department of Applied Physics, University of Santiago de Compostela, 15782, Spain.*
† *Present Address University of Bergen, P.O. Box 7803, N-5020 Bergen, Norway.*
‡These two authors contributed equally.
Email:

Table S1. Suppliers and purities of the chemicals employed in the synthesis of the $[CH_3NH_3][M(HCOO)_3]$ series.

Reagent	Supplier and purity
Metallic Salt:	
$MnCl_2{\cdot}4H_2O$	Sigma-Aldrich ≥98%
$CoCl_2{\cdot}6H_2O$	Sigma-Aldrich 98%
$NiCl_2$	Sigma-Aldrich 98%
$Cu(ClO_4)_2$	Sigma-Aldrich 98%
Organic reagents	
NaHCOO	Sigma-Aldrich ≥99%
CH_3NH_3Cl	Sigma-Aldrich ≥99%
$HCONHCH_3$	Sigma-Aldrich 99%

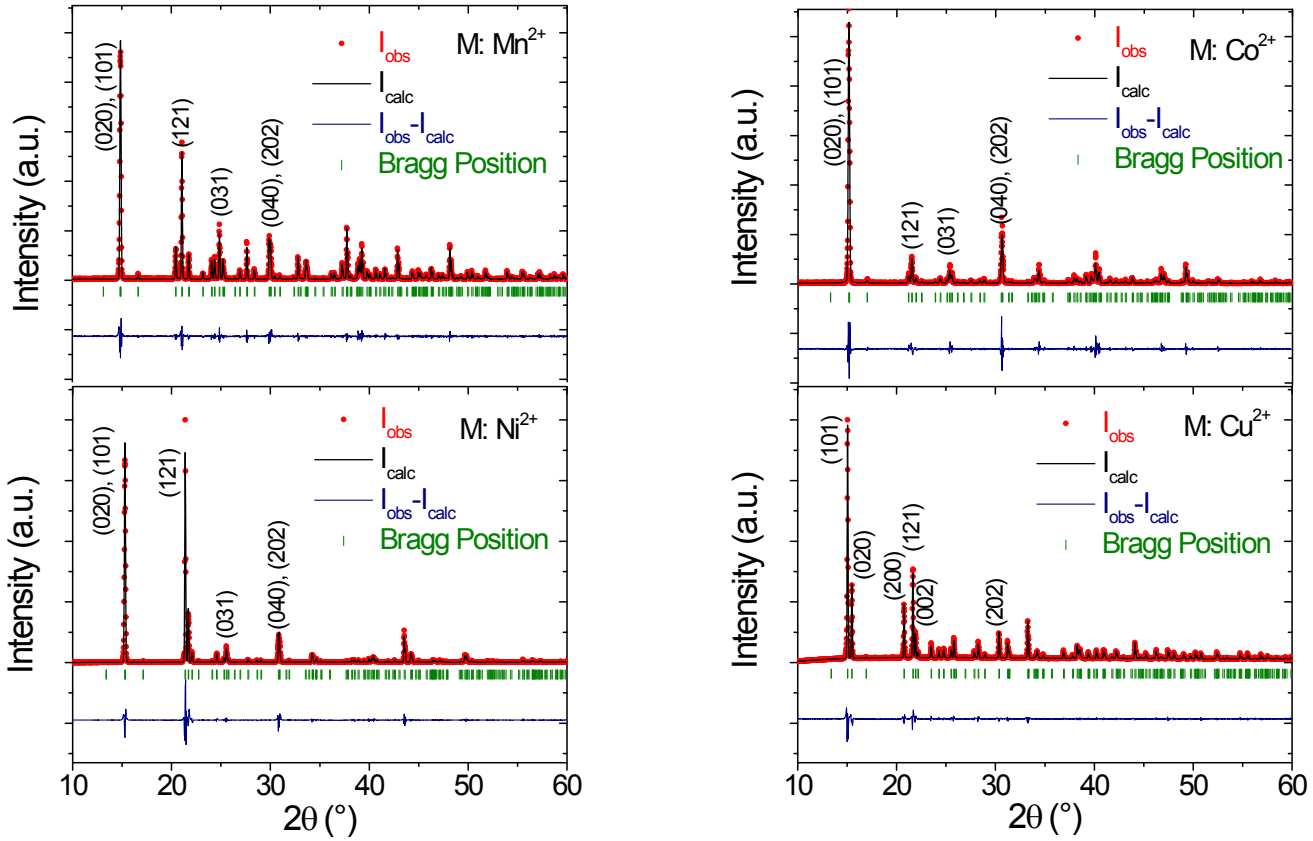

Figure S1. Le Bail refinement of the room temperature PXRD patterns for the $[CH_3NH_3][M(HCOO)_3]$ series. Key: observed data (•) and calculated profile (solid line); the difference plot is drawn below the profile. Tick marks indicate peak positions of the $[CH_3NH_3][M(HCOO)_3]$ phase.

Table S2. $[CH_3NH_3][M(HCOO)_3]$ series cell parameters and cell volume obtained by Le Bail refinements of powder X ray diffraction patterns at room temperature.

$[CH_3NH_3][M(HCOO)_3]$	Cell parameters (Å)			R-factors			
M^{2+}	*a*	*b*	*c*	R_p	R_{wp}	R_{exp}	χ^2
Mn^{2+}	8.6835(1)	11.9512(1)	8.166(1)	12.3	16.6	10.34	2.59
Co^{2+}	8.3911(2)	11.7010(3)	8.1051(2)	18.1	25.0	12.88	3.78
Ni^{2+}	8.3088(1)	11.6001(2)	8.0512(2)	15.8	23.2	17.34	1.79
Cu^{2+}	8.5587(1)	8.110(1)	11.4466(1)	5.98	8.92	9.76	0.84

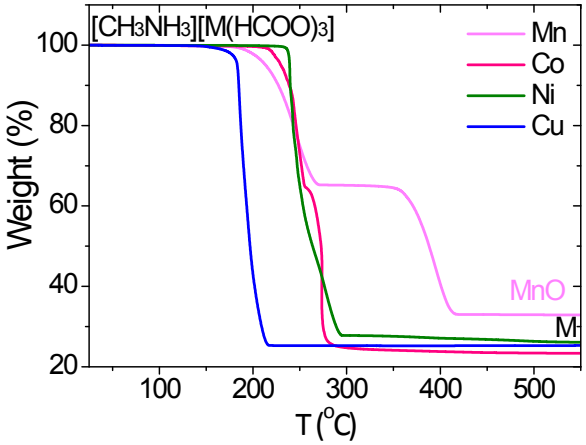

Figure S2a. TGA curves of the $[CH_3NH_3][M(HCOO)_3]$ formates under nitrogen atmosphere

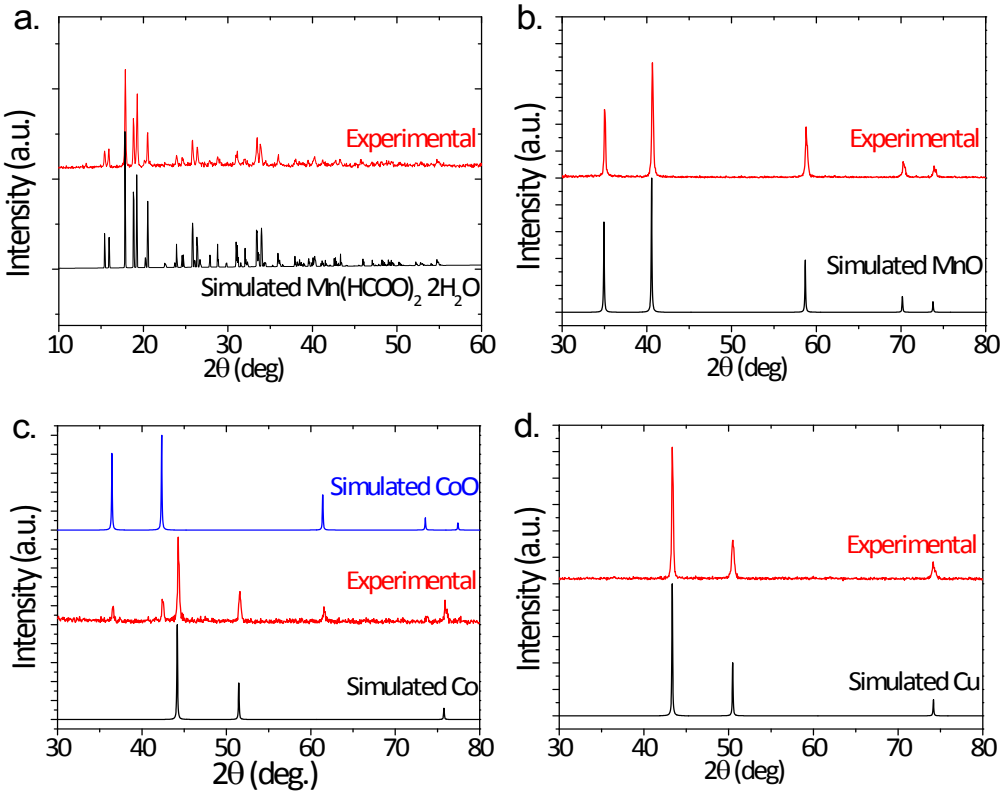

FigureS2b: PXRD patterns of the products obtained after heating these M-MOFs at different temperatures. a) Mn-MOF 300 °C compared with the PXRD simulated for $Mn(HCOO)_2{\cdot}2H_2O$;[1] b) Mn-MOF at 600 °C compared with the PXRD simulated for MnO;[2] c) Co-MOF at 600 °C compared with the PXRD simulated for CoO[3] and Co;[4] d) Cu-MOF at 600 °C compared with the PXRD simulated for Cu.[5]

[1] K. Osaki, Y. Nakai and T. Watanabe, *J. Phys. Soc. Japan*, 1964, **19**, 717–723.
[2] R. E. Pacalo and E. K. Graham, *Phys. Chem. Miner.*, 1991, **18**, 69–80.
[3] A. Taylor and R. W. Floyd, *Acta Crystallogr.*, 1950, **3**, 285–289.
[4] R. W. G. Wyckoff, *Crystal Structures*, Interscience Publishers, New York, 1963, vol. 1
[5] I.-K. Suh, H. Ohta and Y. Waseda, *J. Mater. Sci.*, 1988, **23**, 757–760.

Table S3. Data collection, cell and refinement parameters from the single-crystal X-ray diffraction study of the $[CH_3NH_3][M(HCOO)_3]$ compounds.

Chemical formula	Formula Mass	Crystal system	*a*/Å	*b*/Å	*c*/Å	α, β, γ/°	Unit cell volume/ Å³	T/K	Space group	Z	No. of reflections measured	No. of independent reflections	R_{int}	Final R_1 values ($I > 2\sigma(I)$)	Final $wR(F^2)$ values ($I > 2\sigma(I)$)	Final R_1 values (all data)	Final $wR(F^2)$ values (all data)	Goodness of fit on F^2
$C_4H_9\mathbf{Mn}NO_6$	214.98	Orthorhombic	8.6659(3)	11.9298(3)	8.1529(2)	90.00	842.87(4)	293(2)	Pnma	4	10868	1098	0.0431	0.0524	0.1381	0.0608	0.1464	1.204
$C_4H_9\mathbf{Co}NO_6$	226.05		8.2499(4)	11.6336(6)	8.1398(4)	90.00	781.23(7)	100(2)	Pnma	4	7244	979	0.0539	0.0395	0.1058	0.0490	0.1117	1.071
$C_4H_9\mathbf{Ni}NO_6$	225.83		8.2914(4)	11.5758(6)	8.0379(4)	90.00	771.47(7)	296(2)	Pnma	4	9885	965	0.0404	0.0362	0.0951	0.0472	0.1015	1.221
$C_4H_9\mathbf{Cu}NO_6$	230.66		8.5473(3)	11.4362(4)	8.1022(3)	90.00	791.98(5)	296(2)	Pnma	4	8115	682	0.0458	0.0246	0.0649	0.0348	0.0722	1.076
$C_4H_9\mathbf{Cu}NO_6$	230.66		8.459(5)	11.391(5)	8.133(5)	90.00	783.73(8)	100(2)	Pnma	4	10474	1007	0.0189	0.0230	0.0585	0.0263	0.0609	1.099

Table S4. $[CH_3NH_3][M(HCOO)_3]$ series cell parameters and cell volume obtained by single crystal X ray diffraction at room temperature.

M^{2+}	Ionic radius (Å)	Cell parameters (Å)			Cell volume ($Å^3$)
		a	b	c	
Mn^{2+}	0.83	8.6659(3)	11.9298(3)	8.1529(2)	842.87(4)
[vi]Co^{2+}	0.75	8.4069(9)	11.710(1)	8.1075(9)	798.1(1)
Ni^{2+}	0.69	8.2914(4)	11.5758(6)	8.0379(4)	771.47(7)
Cu^{2+}	0.73	8.5473(3)	11.4362(4)	8.1022(3)	791.98(5)

Table S5. $[CH_3NH_3]M(HCOO)_3$ series M-O and M-M distances (Å), obtained by single crystal X ray diffraction at room temperature.

M^{2+}	Ionic radius (Å)	d_{M-O} (Å)			d_{M-M} (Å)	
		d_a	d_m	d_l	d_1	d_2
Mn^{2+}	0.83	2.173(1)	2.182(1)	2.194(1)	5.9649(2)	5.9491(1)
[i]Co^{2+}	0.75	2.092(2)	2.106(2)	2.116(2)	5.8550(5)	5.8397(4)
Ni^{2+}	0.69	2.056(2)	2.059(2)	2.071(2)	5.7879(3)	5.7740(2)
Cu^{2+}	0.73	1.952(1)	2.008(1)	2.382(1)	5.7181(2)	5.8886(2)

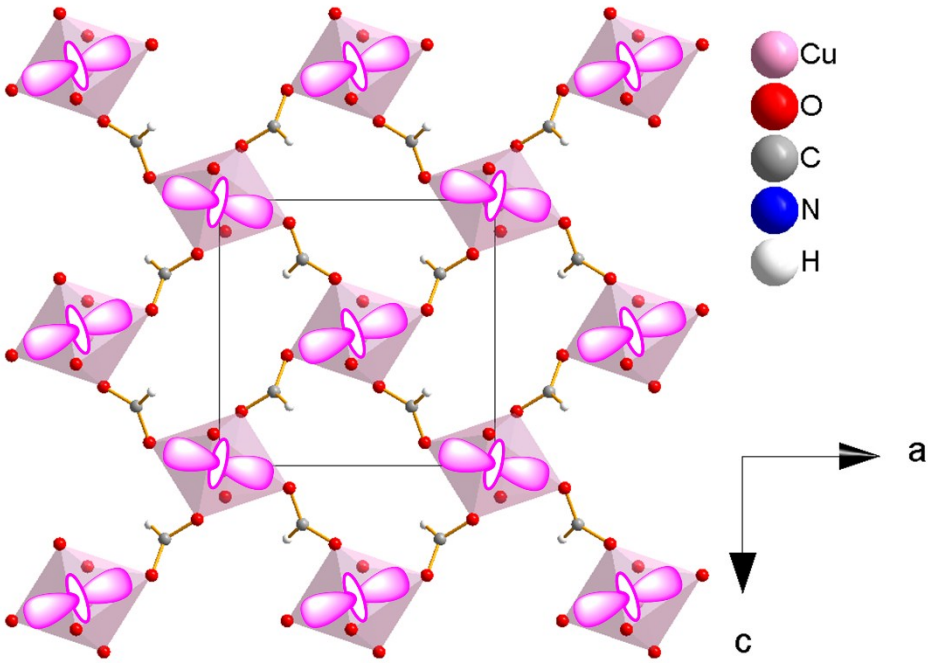

Figure S3. Cooperative orbital ordering of the d_{z^2} orbital within the ac plane in $[CH_3NH_3][Cu(HCOO)_3]$.

[vi] Data taken from M. Boča, I. Svoboda, F. Renz and H. Fuess, *Acta Crystallogr., Sect. C: Cryst. Struct. Commun.*, 2004, **60**, m631–m633.

Table S6. Summary of magnetic properties of $[CH_3NH_3][Mn(HCOO)_3]$ compared with the ones reported in the literature. Curie constant, Curie-Weiss temperature, $\chi_m T$ value, and fitted parameters were calculated from susceptibility data under a 1000 Oe field.

$[CH_3NH_3]Mn(HCOO)_3$	This work	Reference[vii]
T_t / K	8 K	7.8 K
C / cm^3 K mol^{-1}	4.36[a]	4.36
θ/ K	-11.1[a]	-11.2
$\chi_m T$(300K) / cm^3 K mol^{-1}	4.19	4.19
μ_{eff} / μ_B	5.91	5.91
J / cm^{-1}	-0.42[b]	-0.44
g	1.99[b]	2.00
Spin-flop / Tesla	0.60	0.45

a. From the best-fit using Curie-Weiss law (20-300 K, R^2= 0.9998).
b. From the best-fit using Lines model (10-300 K, R^2= 0.9995).

Table S7. Summary of $[CH_3NH_3][Co(HCOO)_3]$ magnetic properties compared with the ones reported in the literature for other perovskite metal–formates with anti–anti formate bridges. Curie constant, Curie-Weiss temperature, $\chi_m T$ value, and fitted parameters were calculated from susceptibility data under a 1000 Oe field.

$[AH]Co(HCOO)_3$	AH:CH_3NH_3	AH[ref.viii]: $(CH_3)_2NH_2$	AH[ref.ix]: $C(NH_2)_3$
T_t / K	15.7	14.9	14.2
C / cm^3 K mol^{-1}	3.42[a]	3.80	3.76
θ / K	-41.3 [a]	-49.4	-53.3
$\chi_m T$ (300K) / cm^3 K mol^{-1}	2.96	3.30	3.19
μ_{eff} / μ_B	5.23	5.52	5.49
J / cm^{-1}	-3.5[b]	-2.3	-4.26
g	2.69 [b]	--	2.80

a. From the best-fit using Curie-Weiss law (20-300 K, R^2= 0.9997).
b. From the best-fit using Lines model (40-300 K, R^2= 0.996).

Table S8. Summary of $[CH_3NH_3][Ni(HCOO)_3]$ magnetic properties compared with the ones reported in the literature for other perovskite metal–formates with anti–anti formate bridges. Curie constant, Curie-Weiss temperature, $\chi_m T$ value, and fitted parameters were calculated from susceptibility data under a 1000 Oe field.

$[AH]Ni(HCOO)_3$	AH: CH_3NH_3	AH[ref.iii]: $(CH_3)_2NH_2$	AH[ref.iv]: $C(NH_2)_3$
T_t / K	34	35	34.2
C / cm^3 K mol^{-1}	1.40[a]	1.27	1.53
θ / K	-64.96 [a]	-55.78	-71.7
$\chi_m T$ (300K) / cm^3 K mol^{-1}	1.15	1.03	1.24
μ_{eff} / μ_B	3.35	3.19	3.50
J / cm^{-1}	-9.38[b]	-4.85	-10.5
g	2.33	--	2.44

a. From the best-fit using Curie-Weiss law (50-300 K, R^2= 0.9997).
b. From the best-fit using Lines model (65-300 K, R^2= 0.996).

Table S9. Summary of $[CH_3NH_3][Cu(HCOO)_3]$ magnetic properties compared with the ones reported in the literature for other perovskite metal–formates with anti–anti formate bridges. Curie constant, Curie-Weiss temperature, $\chi_m T$ value, and fitted parameters were calculated from susceptibility data under a 1000 Oe field.

$[AH][Cu(HCOO)_3]$	AH: CH_3NH_3	AH[ref.iv]: $C(NH_2)_3$
T_t / K	45 & 4	45 & 4.5
C / cm^3 K mol^{-1}	0.49[a]	0.65
θ / K	-59.95 [a]	-87.5
$\chi_m T$ (300K) / cm^3 K mol^{-1}	0.41	0.51
μ_{eff} / μ_B	1.98	2.28
J / cm^{-1}	-48.8 [b]	-47.3
g	2.21 [b]	2.42

a. From the best-fit using Curie-Weiss law (50-300 K, R^2= 0.9997).
b. From the best-fit using Lines model (65-300 K, R^2= 0.996).

[vii] Z. Wang, B. Zhang, T. Otsuka, K. Inoue, H. Kobayashi and M. Kurmoo, *Dalton Trans.*, 2004, 2209–2216

[viii] X.-Y. Y. Wang, L. Gan, S.-W. W. Zhang and S. Gao, *Inorg. Chem.*, 2004, **43**, 4615–4625.

[ix] K.-L. Hu, M. Kurmoo, Z. Wang and S. Gao, *Chem. Eur. J.*, 2009, **15**, 12050–12064.

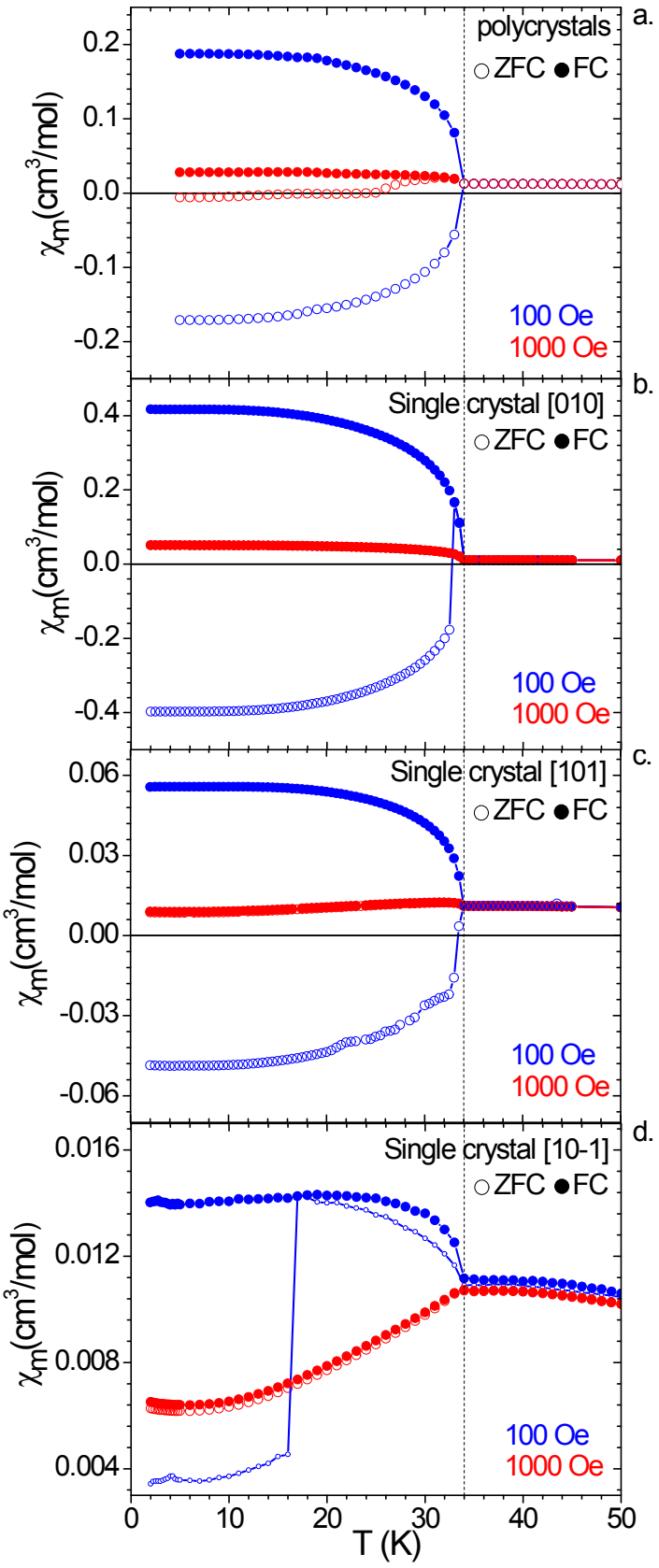

Figure S4. Temperature dependence of χ_m under 100 and 1000 Oe measured in a SQUID under zero-field cooled (ZFC) or field-cooled (FC) conditions for a $[CH_3NH_3][Ni(HCOO)_3]$ polycrystalline sample (a) and single crystal along [010] (b), [101] (c) and [10-1] (d) orientations. The long-range magnetic ordering temperature is indicated by a dashed line.

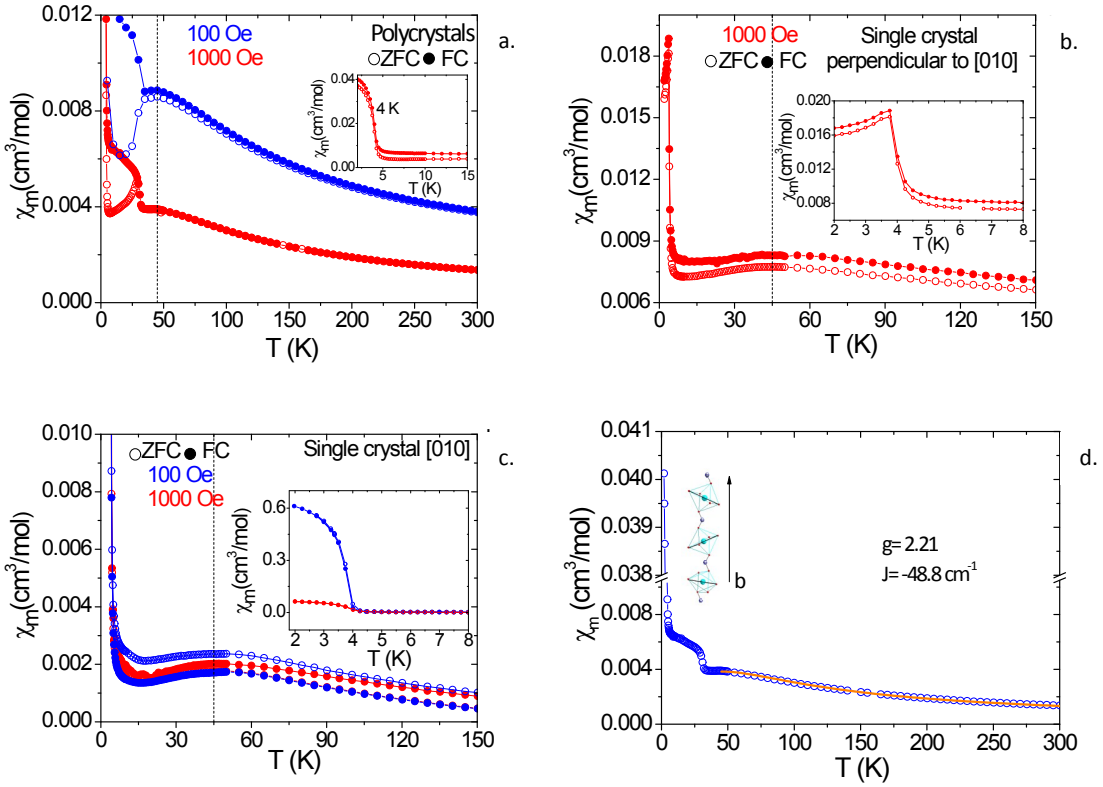

Figure S5. Temperature dependence of χ_m under 100 and 1000 Oe measured in a SQUID under zero-field cooled (ZFC) or field-cooled (FC) conditions for a $[CH_3NH_3][Cu(HCOO)_3]$ polycrystalline sample[x] (a), a single crystal along [010] (b) and a single crystal perpendicular to [010] (d). The long-range magnetic ordering temperature is indicated by a dashed line. Best fit to the Bonner-Fisher model of χ_m for a $[CH_3NH_3][Cu(HCOO)_3]$ powdered sample at H = 1000 Oe under FC conditions (d).

[x] The magnetic susceptibility curve for a polycrystalline sample (Figure S5a) shows three magnetic transitions: the first one as a broad peak around 45 K, the second one as a subtle increase at 35 K, wherein the ZFC and FC curves diverge and the third one as a sharp increase about 4 K, where the curves converge again. Meanwhile in the case of a single crystal, oriented parallel and perpendicular to the [010] direction (Figures S5a and b), two transitions are observed at 45 K and 4 K, furthermore the ZFC and FC curves converge in the whole measured range. These results indicate a strong dependence of the magnetic response on the crystal size, since for the polycrystalline sample an additional transition at 35 K is observed, which could be related with the magnetic response of the particle surface. However, the transitions observed at 45 K and 4 K for both poly and single crystal samples are due to the bulk material.

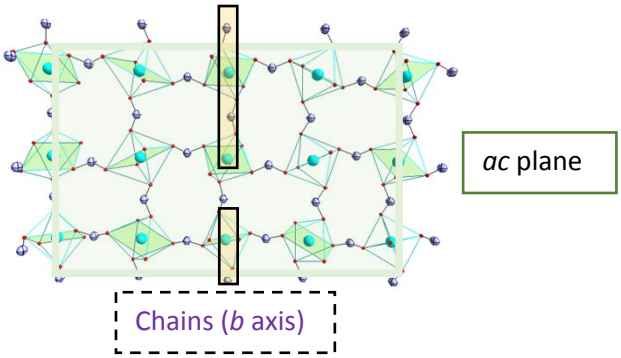

Figure S6. Simplified overview of the magnetic structure of $[CH_3NH_3][Cu(HCOO)_3]$ highlighting the presence chains along the *b* axis.

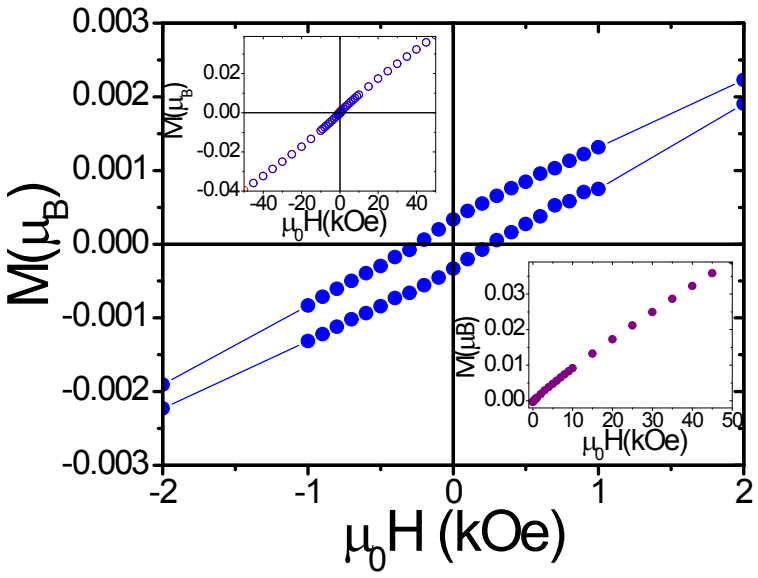

Figure S7. Field-dependent isothermal magnetization *M(T, μ_0H)* for $[CH_3NH_3][Cu(HCOO)_3]$ for a polycrystalline sample at 5 K measured in a SQUID

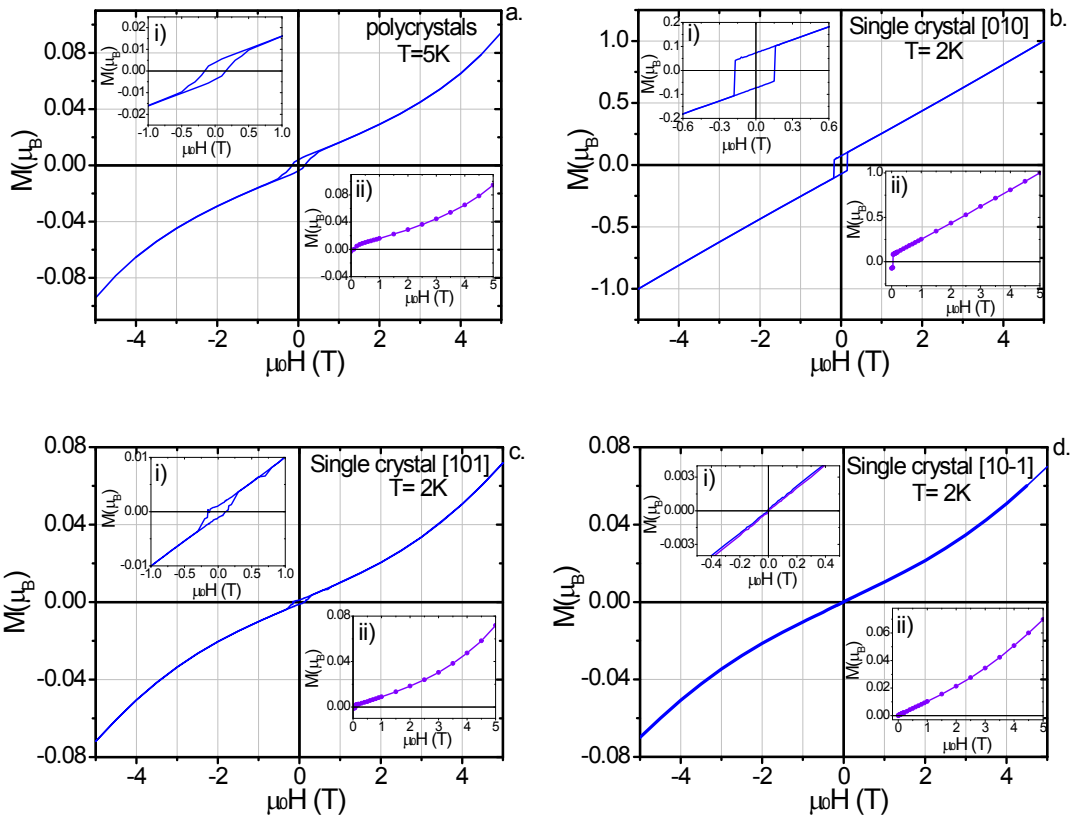

Figure S8. Field-dependent isothermal magnetization *M(T, μ_0H)* for $[CH_3NH_3][Ni(HCOO)_3]$ for a polycrystalline sample at 5 K (a) and a single crystal oriented along [010] (b), [101] (c) and [101] (c) at 2K measured in a SQUID.

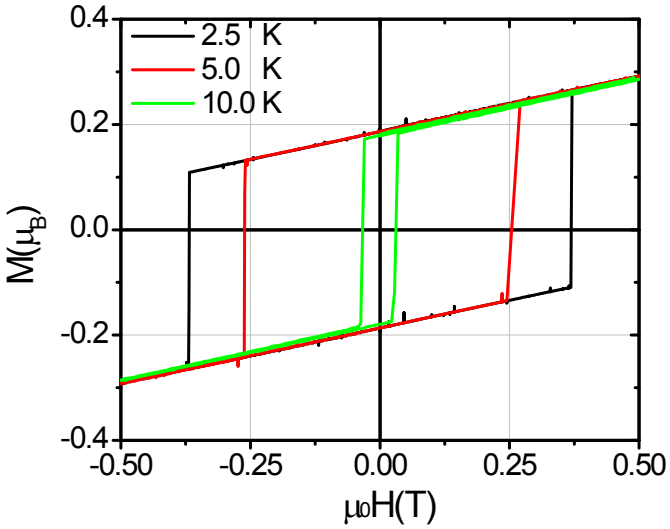

Figure S9. Field-dependent isothermal magnetization *M(T, μ_0H)* for $[CH_3NH_3][Co(HCOO)_3]$ along [010] at different temperatures measured in a VSM.

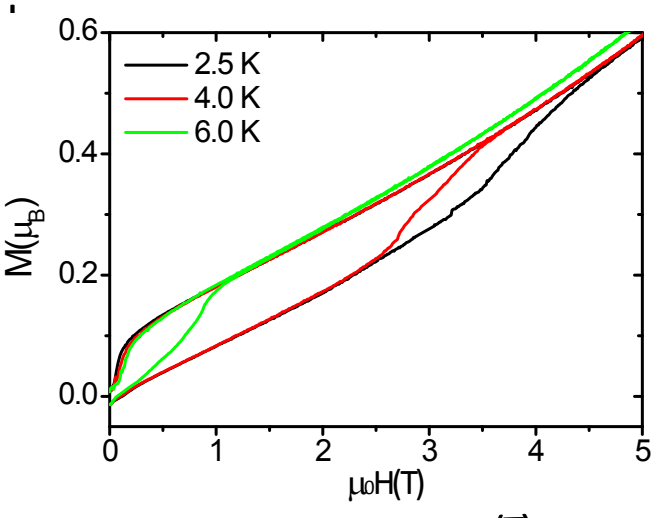

Figure S10. Field-dependent isothermal magnetization *M(T, μ_0H)* for $[CH_3NH_3][Co(HCOO)_3]$ along [101] at different temperatures measured in a VSM.

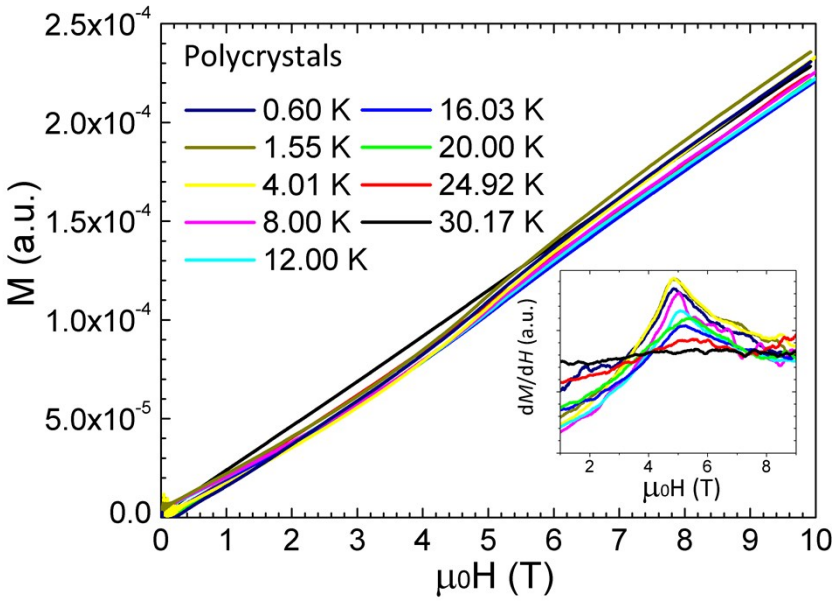

Figure S11. Pulsed field magnetization of a $[CH_3NH_3][Ni(HCOO)_3]$ powdered sample at different temperatures. Inset: derivative of the magnetization.